Aberystwyth University

Prediction of the capillary pressure of fluid surrounding a cylinder representing an idealized rock structure in porous media

Davarpanah, Afshin; Cox, Simon

Regular Article

Prediction of the capillary pressure of fluid surrounding a cylinder representing an idealized rock structure in porous media

Afshin Davarpanah[a], Simon Cox

Department of Mathematics, Aberystwyth University, Aberystwyth SY23 3BZ, UK

© The Author(s) 2022

Abstract Liquids in oil-bearing porous media assume complex shapes that depend on the reservoir characteristics and the wetting properties of the liquid. The wide variation in the geometry of rock formations makes it difficult to accurately predict the capillary pressure of small volumes of liquid and hence the likelihood of being able to move it. Here, we consider the situation in which a small volume of liquid surrounds an upright cylinder on a flat substrate and predict the shape that the liquid takes and its capillary pressure. We validate our predictions by comparing with Surface Evolver simulations for a range of contact angles and cylinder radii.

1 Introduction

The presence of small volumes of a liquid phase in a porous medium is common in processes such as enhanced oil recovery [1], stimulation of plugged wells, environmental remediation [2], and drying via evaporation [3]. Capillary forces can cause the spontaneous imbibition of the liquid phase into micro- or nano-sized pores in porous media, disrupting flow and affecting the efficiency of these processes. Arrays of cylindrical pillars are often used as a canonical example of a microfluidic porous medium [3–5], with the aim of optimizing parameters such as the pressure drop required to mobilize the liquid. It is therefore necessary to have a good understanding of the distribution of liquid in the medium, i.e., both its location and its geometry.

The most important parameter governing the feasibility of, say, oil recovery is the capillary pressure (p_c). This is the difference in pressure between two phases coexisting in the porous medium and depends upon *inter alia*, each phase's volume, relative surface tensions (or contact angles), and pore geometry [6–10]. When regions of different fluids meet, the capillary pressures must equilibrate, and this will determine if the fluid will remain trapped in the complex geometry or whether it can be recovered.

Wetting behavior is described by the contact angle at which interfaces meet, for example between the solid and the liquid and between the air and the liquid. Small contact angles correspond to wetting liquids, with a strong affinity for the substrate, while large contact angles are associated with non-wetting, or hydrophobic, surfaces [11]. Therefore, this parameter has a significant effect on the shape of liquid interfaces in porous media.

The internal geometry of porous media itself may also be difficult to examine and to characterize. For this reason, many studies now turn to manufactured microfluidic geometries to test theories against experiments [4,5,12–15]. One element of such a porous medium might be a solid inclusion that spans the depth of the geometry. For simplicity, we consider such an idealized situation here, described in Sect. 2.1, which allows us to make progress in developing a predictive model for the capillary pressure of a liquid in contact with such an inclusion.

In Sect. 2.3, we derive two approximate solutions of the Young–Laplace equation [7], of increasing complexity, for the capillary pressure of liquid surrounding a cylindrical inclusion, as studied experimentally by Chen et al. [3] in the context of evaporation. We compare this with accurate Surface Evolver simulations, described in Sect. 2.2, to determine its range of validity. In our results (Sect. 3) we explore in particular the effect of different contact angles on the shape and extent of this meniscus for a range of liquid volumes.

The techniques that we use in our derivation are those used to establish the shapes of bubbles [16], menisci [17] and other liquid interfaces in soft matter [18]. More usually, the interface rests on a liquid surface which also deforms [16,19], and it appears that the case considered here, of a liquid meniscus on a solid substrate [20], has received less attention.

---
[a] e-mail: afd6@aber.ac.uk (corresponding author)

2 Geometry and methods

2.1 Geometry

Our idealized porous medium consists of an upright circular cylinder with radius R^* spanning the gap between two flat horizontal parallel surfaces with separation H^*. The gap between the surfaces is filled with air except for a narrow meniscus of liquid around the top and bottom of the cylinder. We assume that the gap between the surfaces is smaller than the capillary length, so that we can neglect the effects of gravity. Since we expect the size of rock pores to be of order microns while the capillary length is of order millimeters, this is likely to be a good approximation. Then by symmetry we need only consider the lower half of this geometry, as shown in Fig. 1, and at such a scale we expect capillary pressures to be of order γ/H^*, where γ is the interfacial tension, of order 30×10^{-3} N/m.

As the liquid volume varies, the capillary pressure will vary from small values at large volumes, where the radius of curvature in the (r, z) plane is large, to much larger values at small volumes. Where the liquid meets the cylinder and where it meets the plate it does so at a particular angle, the contact angle. The contact angle is affected by the properties of the liquid and the surfaces it contacts, so it could be different on the cylinder and the substrate. For simplicity, we take these two values to be the same, but the results described below are straightforward to generalize to the case where they are different.

The contact angle, highlighted in Fig. 1b, is directly related to the balance between the surface tension of the liquid-air interface and the surface tension of the wetting film on the solid walls via the Young equation [11]. If we denote the contact angle by θ_c then

$$\cos \theta_c = \frac{\gamma_w}{\gamma}, \tag{1}$$

where γ_w represents the difference in tension between the unwetted (outer) and wetted (inner) parts of the wall.

The shape of the interface is given by a solution of the Young–Laplace equation [7,21], which balances the capillary pressure with the local mean curvature at each point of the interface. In this cylindrical geometry, the expression for the curvature is highly nonlinear: it has two components, consisting of the principal radii of curvature in two perpendicular directions, and these both vary with vertical position within the meniscus. Our prediction of the capillary pressure will therefore be an approximation, which performs best for large rock structures within the porous medium ($R^* \gg H^*$), and so to determine how accurate our prediction is we will compare it with precise numerical solutions.

2.2 Numerical method

We work in dimensionless coordinates, with all lengths scaled by the gap height H^*. We define the dimensionless cylinder radius to be $R = R^*/H^*$ and choose (without loss of generality) a dimensionless surface tension $\gamma = 1$. Then, a dimensionless capillary pressure of $p_c = 1$ in our results below corresponds to a dimensional capillary pressure of $\gamma/H^* = 30 \times 10^{-3}/10^{-6} = 10^3$Pa.

To perform the simulations we use Surface Evolver [22], which finds the shape of fluid interfaces with given surface tension and other energies under various constraints. Similar calculations have been performed for small pockets of liquid trapped between spheres [23]. The situation that we consider is axisymmetric so that we need only consider the shape of the interface in the (r, z)
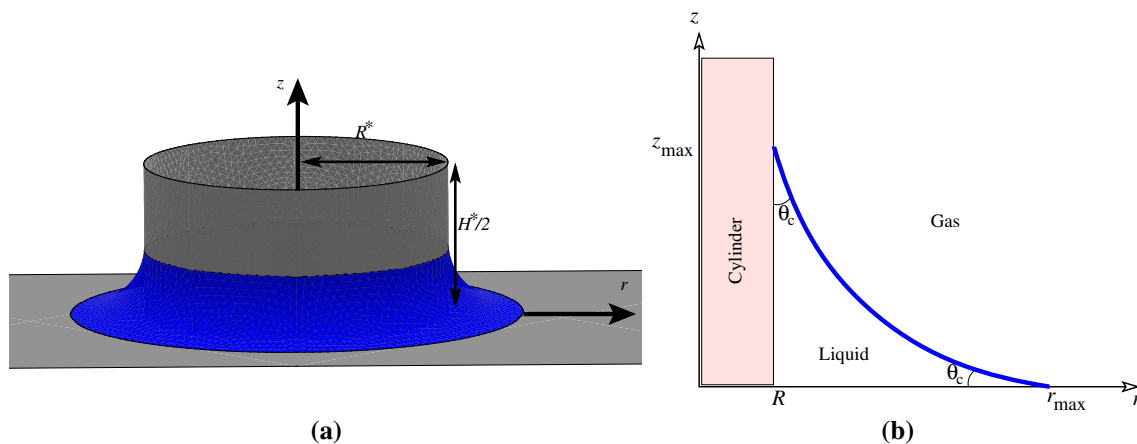
Fig. 1 We seek the shape of a liquid meniscus around the base of a vertical cylinder with circular cross section. **a** 3D view, showing the lower half of the cylinder of radius R^* and height H^*, representing an idealized rock structure in a porous medium, and the liquid meniscus in blue. The wetting films on the cylinder and on the substrate are not shown. **b** Since the meniscus is axisymmetric, it can be described by (dimensionless) radial position r and vertical position z, and we consider only the $r - z$ plane. We consider the case where the contact angles θ_c on the cylinder and the substrate are equal. In this plane the interface has radius of curvature r_c, surface tension γ, extent r_{max} in the radial direction, and height z_{max}

plane (see Fig. 1), which consists of a curve connecting the cylinder to the substrate with the given contact angle at each end and a specified enclosed volume.

This curve is discretized into roughly 2^5 straight elements. The contact angles are considered as further energies, and the system is driven to a minimum of energy using a gradient descent method. In the simulations it is straightforward to vary the cylinder radius R, the liquid volume V and the contact angle θ_c to explore all relevant parameters.

2.3 Mathematical models

In this relatively simple geometry, we can derive approximate formulae for the capillary pressure. The Young–Laplace equation for an interface at equilibrium without gravity is

$$p_c = p_{air} - p_{liquid} = \gamma C, \tag{2}$$

in which the mean curvature C of the interface can be written [16]:

$$C = -\left[1 + r_z^2\right]^{-\frac{3}{2}}\left(r_{zz} - \frac{1 + r_z^2}{r}\right), \tag{3}$$

where subscripts denote derivatives. There are two terms here, corresponding to the two radii of curvature of the interface, one around the cylinder and the other perpendicular to it in the $r - z$ plane. Writing $\hat{p}_c$ for p_c/γ leads to the following equation for the capillary pressure:

$$\hat{p}_c = \left[1 + r_z^2\right]^{-\frac{3}{2}}\left(r_{zz} - \frac{1 + r_z^2}{r}\right). \tag{4}$$

Equation (4) is too complex to find a closed-form solution. Instead, we assume that in typical porous media the size of the rock structures is large, $R \gg 1$. We will consider two approximate solutions: the first will neglect the second term entirely, while the second will approximate it.

2.3.1 Approximation 1: interface shape in the limit of large cylinder radius

The second term in the parentheses in Eq. (4), containing the factor $1/r$, will be dominated by the first at large R, and in our first approximation we choose to neglect it. As we shall see below, we are effectively approximating the interface as a circular arc (precisely one-quarter of a circle if $\theta_c = 0$) in the (r, z) plane.

Equation (4) becomes

$$\hat{p}_c = \text{sign}\left(\frac{\pi}{4} - \theta_c\right)\frac{r_{zz}}{\left[1 + r_z^2\right]^{\frac{3}{2}}}, \tag{5}$$

in which $\text{sign}(\pi/4 - \theta_c)$ reflects the fact that, in this approximation, the curvature of the interface will change sign at a contact angle of $\pi/4$. That is, the capillary pressure will go from positive to negative and the liquid pressure will exceed the air pressure.

Following Teixeira et al. [16], we introduce a coordinate θ with $\cot\theta = r_z$ in Eq. (5) to give

$$\hat{p}_c = \text{sign}\left(\frac{\pi}{4} - \theta_c\right)\sin\theta\frac{d\theta}{dz}. \tag{6}$$

Integrating gives the height of the interface in terms of the parameter θ:

$$z(\theta) = \text{sign}\left(\frac{\pi}{4} - \theta_c\right)(\cos\theta_c - \cos\theta)/\hat{p}_c \quad \text{with} \quad \theta \in \left(\theta_c, \frac{\pi}{2} - \theta_c\right), \tag{7}$$

although $\hat{p}_c$ remains unknown at this stage. The maximum height reached by the meniscus on the cylinder occurs when $\theta = \pi/2 - \theta_c$:

$$z_{\max} = \text{sign}\left(\frac{\pi}{4} - \theta_c\right)(\cos\theta_c - \sin\theta_c)/\hat{p}_c. \tag{8}$$

This expression is shown in Fig. 4, which we describe once the value of $\hat{p}_c$ is predicted.

Since the interface is now approximated by an arc of a circle, the maximum extent of the meniscus in the radial direction is

$$r_{\max} = R + (\cos\theta_c - \sin\theta_c)/\hat{p}_c. \tag{9}$$

We now replace θ from Eq. (6) using $\cot\theta = \dfrac{\cos\theta}{\sqrt{1 - \cos^2\theta}} = -r_z$ to find the interface profile $z(r)$. We substitute for $\cos\theta$ from Eq. (7) and integrate

$$-\frac{dr}{dz} = \frac{\cos\theta_c - \hat{p}_c z}{\sqrt{1 - (\cos\theta_c - \hat{p}_c z)^2}} \tag{10}$$

to obtain

$$\left(z - \frac{\cos\theta_c}{\hat{p}_c}\right)^2 + \left(r - \left(R + \frac{\cos\theta_c}{\hat{p}_c}\right)\right)^2 = \frac{1}{\hat{p}_c^2}. \tag{11}$$

Clearly, this is the equation of a circle with radius $1/\hat{p}_c$ and center $(R + r_c, r_c)$, where $r_c = \cos\theta_c/\hat{p}_c$. The radius of curvature increases, and the meniscus gets larger, as the capillary pressure decreases, as expected. As the contact angle changes the center of curvature moves closer to the axes. We next determine the effect on the capillary pressure of changes in the contact angle.

2.3.2 Approximation 1: capillary pressure in the limit of large cylinder radius

Let us assume that R, θ_c and γ are given. We need to find the capillary pressure $\hat{p}_c$ to completely solve the problem, which we do by determining the liquid volume

$$V = 2\pi \int_R^{R+r_c(1-\tan\theta_c)} z(r) r \, dr \tag{12}$$

with $z(r)$ from Eq. (11). The substitution $r = R + r_c \left(1 - \frac{\cos\theta}{\cos\theta_c}\right)$ allows us to resolve the integral:

$$V = 2\pi r_c^2 \left\{ R \left[1 - \tan\theta_c - \frac{\frac{\pi}{4} - \theta_c}{\cos^2\theta_c}\right] + r_c \left[\frac{(1 - \tan\theta_c)^2}{2} - \frac{\frac{\pi}{4} - \theta_c}{\cos^2\theta_c} + \frac{1 - \tan^3\theta_c}{3}\right]\right\}. \tag{13}$$

In keeping with our assumption that R is large, we retain only the first term, proportional to $r_c^2 R$, and neglect the second term proportional to r_c^3:

$$V \approx 2\pi r_c^2 R \left[1 - \tan\theta_c - \frac{\frac{\pi}{4} - \theta_c}{\cos^2\theta_c}\right] = \frac{2\pi R}{\hat{p}_c^2}\left[\cos^2\theta_c - \frac{1}{2}\sin(2\theta_c) + \theta_c - \frac{\pi}{4}\right]. \tag{14}$$

Introducing the function $f(\theta_c) = \cos^2\theta_c - \frac{1}{2}\sin(2\theta_c) + \theta_c - \frac{\pi}{4}$ for the dependence on the contact angle then gives

$$\hat{p}_c \approx \text{sign}\left(\frac{\pi}{4} - \theta_c\right)\sqrt{\frac{2\pi R f(\theta_c)}{V}}, \tag{15}$$

where $2\pi R/V$ is the reciprocal of the cross-sectional area of the meniscus. This dependence on contact angle precisely matches the expression for a straight channel given by Ma et al. [24], who relate the capillary pressure to the area of the cross section of the channel occupied by liquid. An advantage of our expression is that it allows us to relate the capillary pressure to the volume of the cylindrical meniscus, $\hat{p}_c(V)$, rather than its cross-sectional area (which is more difficult to determine in an experiment).

2.3.3 Approximation 2: Interface shape dependent on cylinder radius

In the preceding approximation we completely neglected the second radius of curvature in the Young–Laplace equation to find a closed-form solution of Eq. (4) in the shape of a circle. We now improve upon this prediction by introducing a dependence on the cylinder radius R. We again assume that R is large and replace the radial position r in the denominator of the second term in Eq. (4) with the cylinder radius R to give

$$\hat{p}_c = [1 + r_z^2]^{-\frac{3}{2}}\left(r_{zz} - \frac{1 + r_z^2}{R}\right). \tag{16}$$

This leads to a semi-analytic expression for the quantities of interest. (It is semi-analytic because we have to solve for the capillary pressure numerically, even though we will find closed-form expressions for the shape and extent of the meniscus.)

Proceeding as before, and assuming for the moment that $\hat{p}_c$ is positive, we introduce the coordinate θ: Eq. (16) becomes

$$\hat{p}_c = \sin\theta\left(\frac{d\theta}{dz} - \frac{1}{R}\right), \tag{17}$$

which improves upon Eq. (6). We rearrange this into the more convenient form

$$\frac{dz}{d\theta} = \frac{R\sin\theta}{R\hat{p}_c + \sin\theta}. \tag{18}$$

In the same way we have

$$\frac{dr}{d\theta} = -\frac{R\cos\theta}{R\hat{p}_c + \sin\theta}. \tag{19}$$

These two equations allow us to find the shape of the meniscus implicitly.

Of the two, Eq. (19) can be integrated more easily: using [25, §2.552.2] and evaluating the constant of integration at $r = R$ gives

$$r(\theta; R, \hat{p}_c, \theta_c) = R\left[1 + \ln\left(R\hat{p}_c + \cos\theta_c\right) - \ln\left(R\hat{p}_c + \sin\theta\right)\right]. \tag{20}$$

Hence the maximum extent of the meniscus beyond $r = R$ is

$$r_{\max}(R, p_c, \theta_c) = R\left[1 + \ln\left(R\hat{p}_c + \cos\theta_c\right) - \ln\left(R\hat{p}_c + \sin\theta_c\right)\right], \tag{21}$$

which is equivalent to Eq. (9) in the limit of large R.

We now integrate Eq. (18) using [25, §2.551.2, 2.551.3] and evaluate the constant of integration at $z = 0$. There are now two branches of the solution depending on the value of $R\hat{p}_c$:

$$z(\theta; R, \hat{p}_c, \theta_c) = R\left[\theta - \theta_c\right]$$
$$+ \begin{cases} \dfrac{2R^2\hat{p}_c}{\sqrt{(R\hat{p}_c)^2-1}}\left[\tan^{-1}\left(\dfrac{R\hat{p}_c\tan(\theta_c/2)+1}{\sqrt{(R\hat{p}_c)^2-1}}\right) - \tan^{-1}\left(\dfrac{R\hat{p}_c\tan(\theta/2)+1}{\sqrt{(R\hat{p}_c)^2-1}}\right)\right] & R\hat{p}_c > 1 \\[3ex] \dfrac{2R^2\hat{p}_c}{\sqrt{1-(R\hat{p}_c)^2}}\left[\coth^{-1}\left(\dfrac{R\hat{p}_c\tan(\theta/2)+1}{\sqrt{1-(R\hat{p}_c)^2}}\right) - \coth^{-1}\left(\dfrac{R\hat{p}_c\tan(\theta_c/2)+1}{\sqrt{1-(R\hat{p}_c)^2}}\right)\right] & R\hat{p}_c < 1. \end{cases} \tag{22}$$

This generalizes Eq. (7) to smaller R. The height, $z_{\max}$, of the meniscus is then found by evaluating this expression with $\theta = \frac{\pi}{2} - \theta_c$.

In our first approximation the curvature of the interface changes sign when $\theta_c = \pi/4$. In this second approximation, it is more difficult to predict when this happens since the magnitude of the first term in parentheses in Eq. (17) depends on not only the contact angle but also the liquid volume (and cylinder radius). However, only small changes to the expressions for $r(\theta)$ and $z(\theta)$, are required for them to continue to work: we change the signs in front of the two trigonometric functions in Eq. (20), replace $+1$ with -1 in Eq. (22), and take the absolute value of the capillary pressure in both formulae. In this way, we can extend the prediction to negative $\hat{p}_c$, as shown in subsequent figures.

2.3.4 Approximation 2: capillary pressure dependent on cylinder radius

Before we can compare the interface shapes with the simulations, we need to determine the dependence of the capillary pressure on the volume V of the meniscus (as well as on the parameters R and θ_c). This requires a further integration, for which we have not been able to determine a closed form expression. Instead, we choose to evaluate the following integral numerically:

$$V = 2\pi \int_{\theta_c}^{\pi/2-\theta_c} z(\theta)r(\theta)\frac{\mathrm{d}r}{\mathrm{d}\theta}\mathrm{d}\theta, \tag{23}$$

substituting the appropriate expressions from eqs. (22), (20) and (19), respectively.

The results of evaluating this integral allow us to determine a value for $\hat{p}_c$ corresponding to a particular liquid volume (for any given values of R and θ_c). The dependence of $\hat{p}_c$ on V is shown in Fig. 2: a strong decrease from a large value for small V. We can now determine the interface shape, the extent of the meniscus in each direction ($r_{\max}$ and $z_{\max}$) and the dependence of each of these quantities on cylinder radius and contact angle.

3 Results

It is clear from our first approximation that as the meniscus increases in size the capillary pressure drops. The volume of the meniscus is approximately its cross-sectional area A multiplied by the circumference of the cylinder, $V = 2\pi RA$, so for a larger cylinder radius a given volume of liquid has to spread further around the circumference and its capillary pressure will increase. However, this observation hides the details of the shape and capillary pressure of the meniscus, and in the following we therefore consider liquid volumes that scale with R, with the expectation that the cross section of the meniscus remains roughly constant in shape. That is, we fix the cross-sectional area A of the meniscus, and consider values that are small enough that $z_{\max} < H/2$ so that the liquid regions around the top and bottom of the cylinder never meet.

3.1 Interface shape

Our second approximation for the meniscus profile is found by plotting Eq. (22) against Eq. (20); examples are shown in Fig. 3a in the case $\theta_c = \pi/18$ and $A = 0.5/2\pi$ for different R. The interface does indeed become closer to a circle as R increases, and the first approximation, Eq. (11), works well for R above about 5. The second approximation shows excellent agreement with the Surface Evolver simulation for $R = 1$, even though the premise for that approximation is that R is large.

In Fig. 4 we show the extent of the meniscus, i.e., values of $r_{\max}$ and $z_{\max}$, for different contact angles and cylinder radii. The radial extent of the meniscus $r_{\max}$ appears constant as the radius of the cylinder varies, while as R increases, the height of the meniscus increases toward the prediction of Eq. (8). This circular approximation works well for R greater than about 20, but the
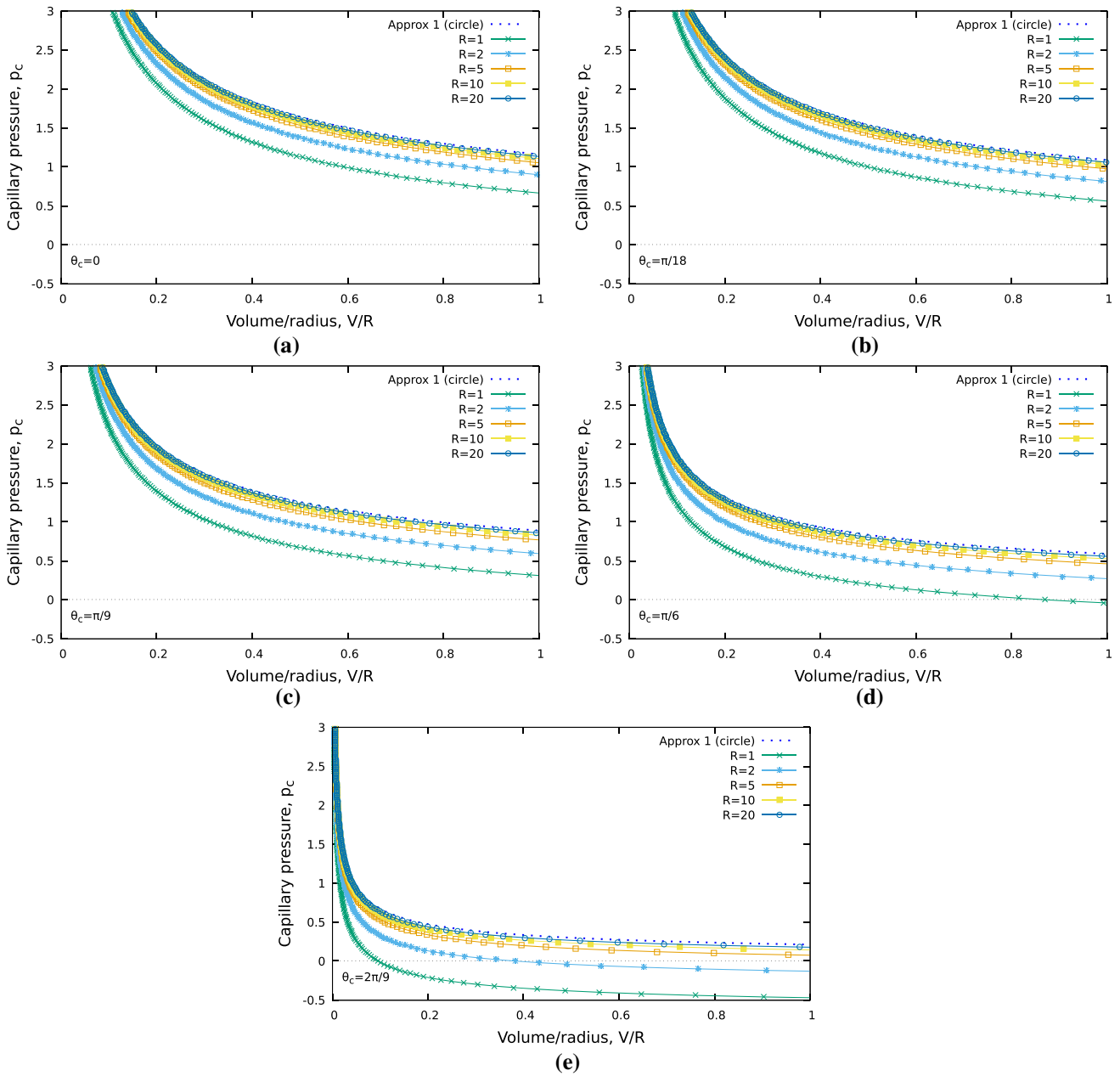
Fig. 2 Profiles of $\hat{p}_c$ against the scaled liquid volume of the meniscus for different values of the cylinder radius R. Each panel is for a different contact angle θ_c. These are numerical integrations of Eq. (23), while the dotted line on each plot is the first approximation, Eq. (15). The horizontal axes are scaled by the cylinder radius R to make the curves comparable, inspired by the form of Eq. (15)

second approximation captures more closely the variation of both z_{max} and r_{max} with R, except for a discrepancy in r_{max} at small R for small contact angles.

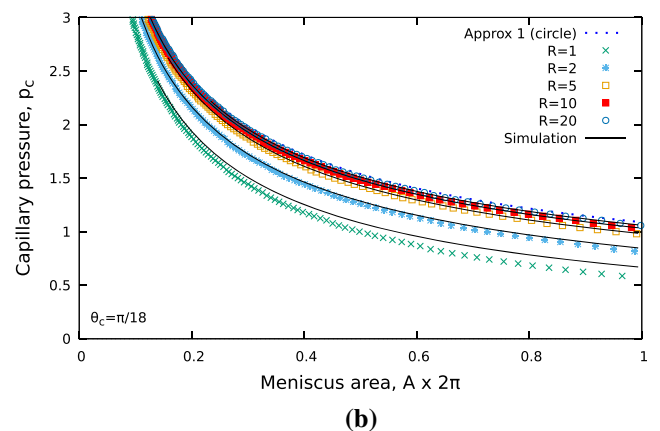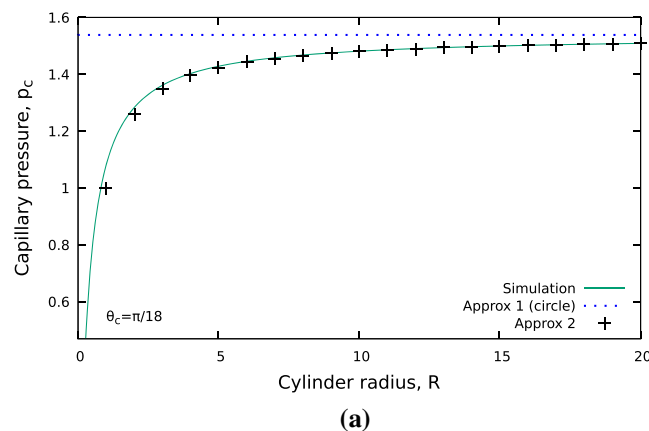### 3.2 Capillary pressure

3.2.1 Effect of cylinder radius

Figure 5a shows that with the meniscus cross-sectional area fixed at $A = 0.5/2\pi$ and the contact angle fixed at $\theta_c = \pi/18$ the capillary pressure increases with R. In this respect, the capillary pressure follows a similar trend to z_{max}: as R increases, the capillary pressure converges toward our first approximation, $\hat{p}_c \approx 1.57$. The second approximation fits the simulated data extremely well, with a small discrepancy only at small R.

Fig. 3 Predicted interface shapes, comparing a circle (our first approximation, Eq. (11), dotted line), the second approximation (eqs. (20) and (22), solid lines) and Surface Evolver simulations. In each case the liquid area is $A = 0.5/2\pi$ and the appropriate value of $\hat{p}_c$ for the second approximation is chosen from the profiles in Figure 2. **a** Profiles in the $r-z$ plane for different cylinder radii R and contact angle $\theta_c = \pi/18$. The simulation data for $R = 1$ is shown as a dashed line. **b** Profiles in the $r-z$ plane for different contact angles θ_c and radius $R = 1$. The simulation data is shown as solid black lines that overlay the predictions


(a)

(b)

(a)

(b)
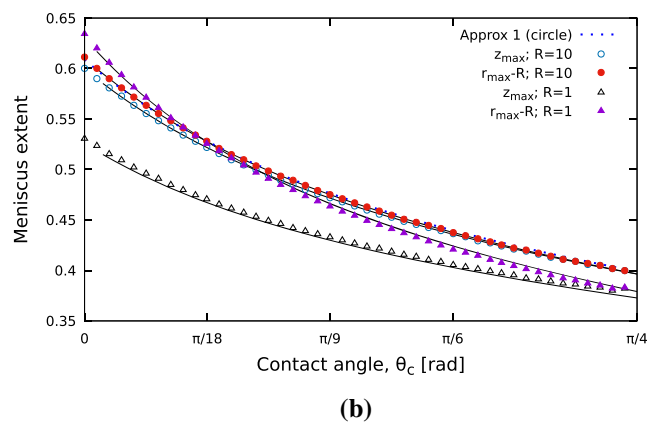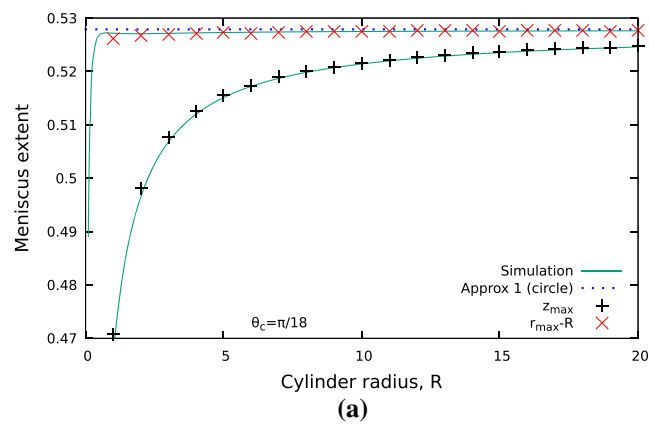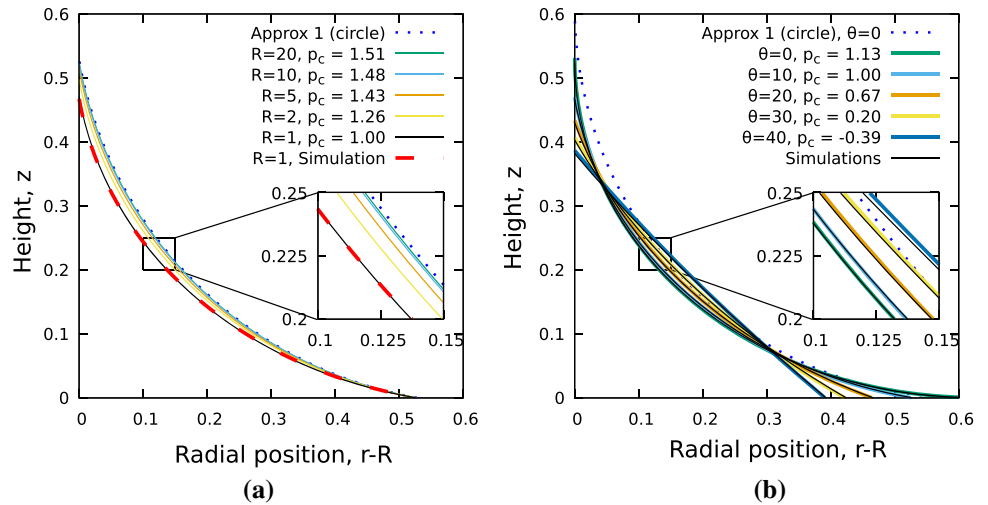
Fig. 4 Predicted values of the extent of the meniscus in the radial ($r_{max} - R$) and vertical (z_{max}) directions compared with Surface Evolver simulations. **a** With contact angle $\theta_c = \pi/18$ and liquid area $A = 0.5/2\pi$, as in Fig. 3, the first approximation (eqs. (9) and (8) with $\hat{p}_c$ from Eq. (15), shown as a horizontal dotted line) is independent of radius R, while the second approximation (eqs. (21) and (22), shown as points) match the simulated data (solid lines) for R greater than one. Note how little the value of r_{max} varies with cylinder radius R. **b** The dependence of the extent of the meniscus in the r and z directions on the contact angle θ_c is shown for $R = 1$ and $R = 10$. The simulated data (solid lines) is in good agreement with the second approximation for both values of R over a wide range of contact angles, while the first approximation is in broad agreement with the data for both r_{max} and z_{max} only for large R and large θ_c

(a)

(b)

Fig. 5 Effect of cylinder radius on capillary pressure. **a** Comparing simulated data (solid line) with our first (horizontal dotted line) and second (points) approximations for constant meniscus area $A = 0.5/2\pi$ and contact angle $\theta_c = \pi/18$. **b** Capillary pressure for a range of areas A (multiplied by 2π) and cylinder radii R, with contact angle $\theta_c = \pi/18$, as in Fig. 2b. Simulated data is shown as solid lines, showing better agreement at larger R and smaller θ_c
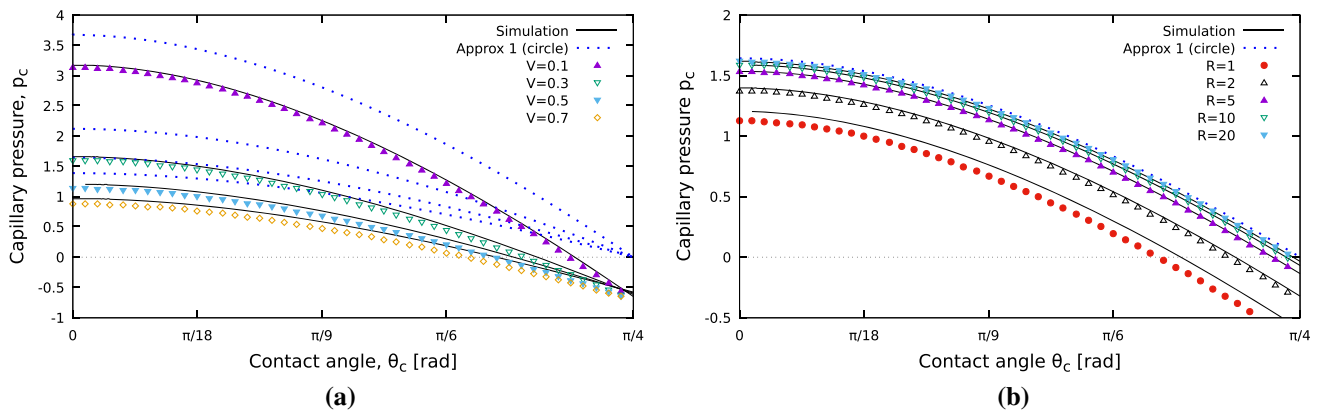
Fig. 6 Effect of contact angle and meniscus size on capillary pressure, comparing simulated data (solid lines) with our first (blue dotted lines) and second approximations (points). **a** For different meniscus volumes with cylinder radius $R = 1$. **b** For different cylinder radii R and meniscus area $A = 0.5/2\pi$

Again for $\theta_c = \pi/18$, Fig. 5b shows the capillary pressure for a range of values of the liquid cross-sectional area, comparing the predictions with simulated data. For each value of R, the capillary pressure decreases as the meniscus area increases, most steeply for small liquid areas and small cylinder radii. Although the first approximation works well for large R (here $R = 20$), the second approximation performs better down to lower values of R.

3.2.2 Effect of contact angle

Representative interface shapes are shown in Fig. 3b for different contact angles. As the contact angle increases, the curvature reduces, and hence so does the capillary pressure.

The same trend of decreasing capillary pressure with increasing volume is observed for all contact angles and all meniscus volumes (Fig. 6a). The highest capillary pressures are found for the smallest contact angles, since as the contact angle increases, the interface straightens out, and for the smallest liquid volumes, since the interface is more strongly curved closer to the cylinder. For $R = 1$ the second approximation works well, more so at smaller liquid volumes/higher capillary pressures.

Figure 6b shows that our first approximation of the capillary pressure is indistinguishable from the data for all values of the contact angle for large cylinders (R above about 20). The second approximation works much better at lower R, although for R as low as one there is a discrepancy of about 10%, almost independent of the contact angle.

For certain values of the contact angle and liquid volume the capillary pressure (and hence the curvature of the interface) can change sign; an example is shown in Fig. 6a for $R = 1$ and θ_c greater than $\pi/6$. When the capillary pressure is zero the meniscus takes the form of a catenoid, with equation

$$z = R \cos \theta_c \left[\cosh^{-1} \left(\frac{1}{\sin \theta_c} \right) - \cosh^{-1} \left(\frac{r}{R \cos \theta_c} \right) \right]. \tag{24}$$

Determining the volume in this case, using the integral in Eq. (12) with upper limit $R/\tan \theta_c$, shows that the value of θ_c at which the capillary pressure is zero decreases as the liquid volume increases, while for fixed volume it converges on $\pi/4$ as R increases. Thus, for sufficiently small volumes the critical contact angle at which the capillary pressure changes sign is still $\pi/4$.

Figure 6a also suggests that there is a particular contact angle at which the capillary pressure is independent of the liquid volume for given radius R. This occurs at $\theta_c = \pi/4$ for large R, since the interface is flat (in the (r, z) plane). For smaller R, it occurs at negative capillary pressure ($\hat{p}_c \approx -0.5$ for $R = 1$), so that the interface curvature has changed sign and it bulges outwards slightly. The critical contact angle at which $\hat{p}_c(\theta_c)$ converges remains very close to $\theta_c = \pi/4$.

4 Discussion and conclusions

We have described numerical simulations and two predictive models for the shape of the meniscus surrounding the base of a circular cylinder attached to a flat horizontal substrate. In many ways this is simpler than the more familiar problem of the capillary rise of liquid around a bubble at the surface of a liquid [16,17], and the different boundary condition at $r_{\max}$ allows us to make progress with (i) a closed-form solution that works well at large R, i.e., cylinders that are many times wider than their height, and (ii) semi-analytic solutions that works well for a much broader range of values of R, showing significant error only at large liquid volumes (when gravity might be anticipated to have a further significant effect) and small R less than one. In this second approximation, Fig. 2 shows how the capillary pressure depends on liquid volume, removing the need for numerical calculations, with eqs. (20) and (22) giving the shape of the meniscus.

Notable features of the solutions we give are:

- The radial extent of the meniscus is much better described than the meniscus height by our first approximation, while the second approximation captures both well; indeed, the radial extent of the meniscus appears almost independent of cylinder radius for fixed cross-sectional area (Fig. 4a) down to R below 1 (in units of the channel depth);
- the critical contact angle at which the interface curvature/capillary pressure is zero decreases as the cylinder radius decreases and as the meniscus volume increases (Fig. 6);
- there appears to be a particular contact angle at which the capillary pressure is the same, irrespective of the meniscus volume, for given cylinder radius (Fig. 6a).

By establishing predictive models for the capillary pressure in this idealized geometry, we aim to provide quantitative results to enable comparison with experiment. Providing results for capillary pressure and interface shape for a broader range of geometries, for example cylindrical pillars with small radius R, different shapes of pillars, or more than one pillar, is the subject of ongoing research.

References

1. L.W. Lake, R.T. Johns, W.R. Rossen, G.A. Pope, *Fundamentals of enhanced oil recovery* (Society of Petroleum Engineers, Richardson, 2014)
2. I. Cantat, S. Cohen-Addad, F. Elias, F. Graner, R. Höhler, O. Pitois, F. Rouyer, A. Saint-Jalmes, *Foams: structure and dynamics* (OUP Oxford, Oxford, 2013)
3. C. Chen, P. Duru, P. Joseph, S. Geoffroy, M. Prat, Control of evaporation by geometry in capillary structures. From confined pillar arrays in a gap radial gradient to phyllotaxy-inspired geometry. Scientif. Rep. **7**, 15110 (2017)
4. D. Horner, S. Ravi, S. Moghaddam, Monoporous micropillar wick structures, II-optimization & theoretical limits. Appl. Thermal Eng. **73**, 1378–1386 (2014)
5. C. Byon, S.J. Kim, The effect of meniscus on the permeability of micro-post arrays. J. Micromech. Microeng. **21**, 115011 (2011)
6. S.M. Hassanizadeh, W.G. Gray, Thermodynamic basis of capillary pressure in porous media. Water Resour. Res. **29**, 3389–3405 (1993)
7. G. Soligno, M. Dijkstra, R. van Roij, The equilibrium shape of fluid-fluid interfaces: Derivation and a new numerical method for Young's and Young-Laplace equations. J. Chem. Phys. **141**, 244702 (2014)
8. T.S. Wong, T. Sun, L. Feng, J. Aizenberg, Interfacial materials with special wettability. MRS Bull. **38**, 366–371 (2013)
9. J.S. Rowlinson, B. Widom, *Molecular theory of capillarity* (Dover, New York, 2013)
10. W. Xu, J.T. Ok, F. Xiao, K.B. Neeves, X. Yin, Effect of pore geometry and interfacial tension on water-oil displacement efficiency in oil-wet microfluidic porous media analogs. Phys. Fluids **26**, 093102 (2014)
11. P.G. De Gennes, F. Brochard-Wyart, D. Quéré, *Capillarity and wetting phenomena: drops, bubbles, pearls, waves* (Springer, New York, 2004)
12. R. Xiao, R. Enright, E.N. Wang, Prediction and optimization of liquid propagation in micropillar arrays. Langmuir **26**, 15050–15075 (2010)
13. S.W. Jeong, M.Y. Corapcioglu, A micromodel analysis of factors influencing NAPL removal by surfactant foam flooding. J. Contam. Hydrol. **60**, 77–96 (2003)
14. J. Cui, T. Babadagli, Use of new generation chemicals and nano materials in heavy-oil recovery: visual analysis through micro fluidics experiments. Coll. Surf. A: Physicochem. Eng. Aspects **529**, 346–355 (2017)
15. M. Haghighi, B. Xu, Y.C. Yortsos, Visualization and simulation of immiscible displacement in fractured systems using micromodels: I. Drainage. J. Coll. Interf. Sci. **166**, 168–179 (1994)
16. M.A. Teixeira, S. Arscott, S.J. Cox, P.I. Teixeira, What is the shape of an air bubble on a liquid surface? Langmuir **31**, 13708–13717 (2015)
17. P.D. Howell, The draining of a two-dimensional bubble. J. Eng. Math. **35**, 251–272 (1999)
18. V.N. Paunov, P.A. Kralchevsky, N.D. Denkov, I.B. Ivanov, K. Nagayama, Capillary meniscus interaction between a microparticle and a wall. Coll. Surf. **67**, 119–138 (1992)
19. C. Pozrikidis, Shape of hexagonal hydrostatic menisci. Intl. J. Numer. Methods Fluids **65**, 625–637 (2011)
20. M.A. Teixeira, S. Arscott, S.J. Cox, P.I. Teixeira, When is a surface foam-phobic or foam-philic? Soft Matter **14**, 5369–5382 (2018)
21. A. Yeung, T. Dabros, J. Masliyah, Dissipative Interfaces and Departures from the Young-Laplace Equation. Langmuir **13**, 6597–6606 (1997)
22. K.A. Brakke, The Surface Evolver. Exp. Math. **1**, 141–165 (1992)
23. J.L. Hilden, K.P. Trumble, Numerical analysis of capillarity in packed spheres: planar hexagonal-packed spheres. J. Coll. Interf. Sci. **267**, 463–474 (2003)
24. S. Ma, G. Mason, N.R. Morrow, Effect of contact angle on drainage and imbibition in regular polygonal tubes. Coll. Surf. A: Physicochem. Eng. Aspects **117**, 273–291 (1996)
25. I.S. Gradshteyn, I.M. Ryzhik, *Table of integrals, series, and products* (Academic Press, New York, 1980)